JOURNAL OF VIROLOGY, Sept. 2008, p. 8721–8732 Vol. 82, No. 17
0022-538X/08/$08.00+0 doi:10.1128/JVI.00818-08

Pathways of Cross-Species Transmission of Synthetically Reconstructed Zoonotic Severe Acute Respiratory Syndrome Coronavirus▽

Timothy Sheahan,[1] Barry Rockx,[2] Eric Donaldson,[1] Davide Corti,[3] and Ralph Baric[1,2]*

Department of Microbiology and Immunology, University of North Carolina at Chapel Hill, Chapel Hill, North Carolina[1]; Department of Epidemiology, University of North Carolina at Chapel Hill, Chapel Hill, North Carolina[2]; and Institute for Research in Biomedicine, Bellinzona, Switzerland[3]

Received 16 April 2008/Accepted 16 June 2008

Zoonotic severe acute respiratory syndrome coronavirus (SARS-CoV) likely evolved to infect humans by a series of transmission events between humans and animals in markets in China. Virus sequence data suggest that the palm civet served as an amplification host in which civet and human interaction fostered the evolution of the epidemic SARS Urbani strain. The prototypic civet strain of SARS-CoV, SZ16, was isolated from a palm civet but has not been successfully cultured in vitro. To propagate a chimeric recombinant SARS-CoV bearing an SZ16 spike (S) glycoprotein (icSZ16-S), we constructed cell lines expressing the civet ortholog (DBT-cACE2) of the SARS-CoV receptor (hACE2). Zoonotic SARS-CoV was completely dependent on ACE2 for entry. Urbani grew with similar kinetics in both the DBT-cACE2 and the DBT-hACE2 cells, while icSZ16-S only grew in DBT-cACE2 cells. The SZ16-S mutant viruses adapted to human airway epithelial cells and displayed enhanced affinity for hACE2 but exhibited severe growth defects in the DBT-cACE2 cells, suggesting that the evolutionary pathway that promoted efficient hACE2 interactions simultaneously abolished efficient cACE2 interactions. Structural modeling predicted two distinct biochemical interaction networks by which zoonotic receptor binding domain architecture can productively engage hACE2, but only the Urbani mutational repertoire promoted efficient usage of both hACE2 and cACE2 binding interfaces. Since dual species tropism was preserved in Urbani, it is likely that the virus evolved a high affinity for cACE2/hACE2 receptors through adaptation via repeated passages between human and civet hosts. Furthermore, zoonotic SARS-CoV was variably neutralized by antibodies that were effective against the epidemic strain, highlighting their utility for evaluating passive immunization efficacy.

Within the wet markets in China, a wide range of common and exotic food animals like bats and civets are sold live or as fresh meat for human consumption, in part to improve health and for sexual performance (2, 8, 32, 34). In southern China, the consumption of exotic animals is especially common during the winter months when most respiratory tract infections are highly prevalent (32). Since many zoonotic viral pathogens are shed in stool, densely housed birds and mammals shedding excreta in the wet marketplace create a rich atmosphere for zoonotic virus transmission to human consumer populations (32). Most recently, wet markets in Southeast Asia have been associated with cultivating the cross-species transmission of avian influenza H5N1 and the newly emerged severe acute respiratory syndrome coronavirus (SARS-CoV) (8, 13, 32).

In 2002, a novel coronavirus, SARS-CoV, emerged as the causative agent of severe acute respiratory syndrome and spread worldwide, causing about 8,000 cases and more than 700 deaths (3, 23, 32). Viruses similar to the epidemic strain SARS-CoV Urbani were isolated from animals for sale within wet markets in China during the epidemic in 2003 and the reemergence in 2004 (2, 8). Genome sequences of viruses isolated from bats, civets, and humans suggest that viruses circulating in bats crossed the species barrier to infect civets, which then served as an amplification host for yet another host range shift to generate a human-tropic virus (2, 8, 13, 19). Recent surveys of animal populations in North America, Africa, and China implicate bats as reservoirs of a diverse array of coronaviruses, including SARS-CoV-like progenitors (5, 6, 13, 14, 20, 31–33). As some bat species were found to be coinfected with more than one coronavirus lineage, the recombination between and within genogroups and the subsequent emergence of novel coronaviruses are real possibilities (14). In 2007, surveys of wild Asian leopard cats and Chinese ferret badgers revealed the presence of yet more novel and highly divergent coronaviruses circulating in animals typically sold in wet markets in China (6). Since viruses similar to the epidemic strain of SARS-CoV are currently circulating in zoonotic pools, the future emergence of another SARS-CoV-like virus may occur. Therefore, it is imperative that current vaccination and passive immunization therapies are effective in protecting humans from infection by a wide range of epidemic and zoonotic SARS-CoV. Unfortunately, bat SARS-CoV and the prototypical civet SARS-CoV strain SZ16 have not been successfully cultured in vitro, hampering our ability to evaluate their epidemic potential, pathogenesis, and susceptibility to current therapeutic interventions within in vitro and in vivo models (13, 15).

The SARS-CoV spike (S) gene sequences isolated from human cases during the early phase of the epidemic in 2002 to 2003 and during the reemergence from 2003 to 2004 are very similar to those of the SZ16 strain (2, 8, 12). SZ16 was isolated from the palm civet in wet markets within the Guangdong

* Corresponding author. Mailing address: Department of Epidemiology, 2107 McGavran-Greenberg, CB no. 7435, University of North Carolina, Chapel Hill, NC 27699-7435. Phone: (919) 966-3895. Fax: (919) 966-2089. E-mail: rbaric@email.unc.edu.

▽ Published ahead of print on 25 June 2008.

region of China during the epidemic, and its S protein differs from the that of the epidemic strain by 18 amino acids, 16 of which reside in the S1 domain containing the receptor binding domain (RBD) (8). The SARS-CoV strain GD03 sequence was isolated from a sporadic human case during the epidemic's reemergence in 2003 to 2004 and closely resembles those viruses isolated from civets and raccoon dogs from the wet markets (2). The SARS-CoV GD03 S protein differs from that of the epidemic strain by 17 amino acids, 16 of which reside in the S1 domain (2). Recently, we have shown that the recombinant SARS-CoV bearing the SZ16 S gene (icSZ16-S) was capable of replication within Vero E6 cells, but progeny virions were unable to infect naïve cell cultures, supporting evidence that the binding of the civet S protein to the human SARS-CoV receptor (human angiotensin-converting enzyme II [hACE2]) or a very closely related primate ortholog was inefficient (19). Since clinical SZ16 isolates and our recombinant chimeric icSZ16-S virus strains could not be successfully cultured in vitro, the biology of the SZ16 S protein and its effect on virus growth and pathogenesis remain elusive.

In this study, we describe the recovery and growth of the icSZ16-S strain in culture using delayed brain tumor (DBT) cells stably expressing the civet ortholog (cACE2) of hACE2. Like the epidemic strain, and in contrast to an earlier report, both icSZ16-S and icGD03-S are completely dependent on ACE2 for entry (36). In DBT-cACE2 cells, icSZ16-S grows with kinetics similar to that of the epidemic strain, but point mutations in the SZ16 S glycoprotein that enhance growth in hACE2-expressing cells abrogate growth in cACE2-expressing cells. The epidemic strain grows equally well in cACE2- and hACE2-expressing cells, suggesting that the epidemic strain probably evolved through repeated exchanges of virus between civet and human, thereby providing the evolutionary pressure to retain dual host tropism. icSZ16-S and icGD03-S are moderately susceptible to neutralization by the human monoclonal antibody (hu-MAb) S230.15. Unlike the epidemic strain, zoonotic viruses are resistant to hu-MAb S3.1, suggesting that therapeutics successfully directed against the epidemic strain may not work as well against the zoonotic viruses. These data highlight the utility of employing an antigenically diverse zoonotic S panel of SARS-CoV in the study of host range expansion and antiviral therapy efficacy.

MATERIALS AND METHODS

Viruses and cells. The recombinant epidemic virus strain "icSARS" (GenBank accession no. AY278741) and icSZ16-S (GenBank accession no. AY304488), icGD03-S (GenBank accession no. AY525636), icCUHK-W1 (GenBank accession no. AY278554), icGZ02 (GenBank accession no. AY390556), icSZ16-S K479N, icSZ16-S K479N D8, and icSZ16-S K479N D22 were propagated on Vero E6 or DBT cells stably expressing cACE2 (DBT-cACE2) as described previously (4, 22, 25, 26, 37). The icSZ16-S virus supernatant from the electroporated cell culture (passage 0) was passaged on DBT-cACE2 cells four times at 48-h intervals, after which a robust cytopathic effect was observed. icSZ16-S was then plaque purified on DBT-cACE2 cells, and plaques were expanded in six-well dishes of DBT-cACE2 cells. Six-well-dish supernatant was used to infect a T175 flask of DBT-cACE2 cells to generate a virus stock that was harvested 20 h postinfection (hpi). Viral RNA from the icSZ16-S virus stock was isolated using TRIzol (Invitrogen, Carlsbad, CA), cDNA was synthesized using Superscript II reverse transcriptase (SSII; Invitrogen, Carlsbad, CA), and amplicons spanning the S, 3a, E, and M genes were generated by reverse transcription-PCR (RT-PCR) and sequenced directly. The virus stocks used throughout this study were grown and titers were determined by plaque assay with Vero E6 and/or DBT-cACE2 cells as described previously (38). Vero E6 and DBT cells were grown in minimal essential medium (Invitrogen, Carlsbad, CA) supplemented with 10% Fetal Clone II (HyClone, South Logan, UT), kanamycin (0.25 μg/ml), and gentamycin (0.05 μg/ml) (UNC tissue culture facility). DBT-cACE2 and DBT-hACE2 cells were grown in Vero/DBT growth media supplemented with 700 μg/ml G418 (Invitrogen, Carlsbad, CA). All work with viruses was performed in a class II biological safety cabinet in a certified biosafety level 3 laboratory containing redundant exhaust fans while wearing Tyvek suits and powered air-purifying respirators as described previously (38).

Generation of cACE2-expressing DBT cells. Plasmids encoding N-terminal Myc-tagged hACE2 and cACE2 were kindly provided by M. Farzan, New England Primate Research Center. Construction of the DBT-hACE2 cell line was carried out as described by Sheahan et al. (26). The cACE2 gene was amplified by PCR using Expand High Fidelity polymerase (cACE2F primer, 5′-CACCATGTCAGGCTCTTTCTGGCTCC-3′; and cACE2R primer, 5′-AAATGAAGTCTGAACGTCATCAG-3′). Amplicon was gel purified and cloned into pcDNA3.1/V5-His according to the protocol. The cACE2 reverse primer did not contain a stop codon, allowing for a read through and the inclusion of a six-His tag on the 3′ end. The pcDNA cACE2-His plasmids were sequenced and found to have two amino acid changes, G354D and R736Q, compared to those of the published sequence (GenBank accession no. AY881174), one of which (G354D) resides at a proposed interaction site with SARS-CoV S residues Y491 and G488, but these changes were also found in the parent gifted plasmid. cACE2 is polymorphic at residue 354, where sequences containing D354 and G354 can be found in civet tissue samples (personal communication with Michael Farzan) (18). Murine DBT cells were transfected with 4 μg of pcDNA3.1/V5-His expressing cACE2-His or green fluorescent protein (GFP)-His, using Fugene reagent (Roche, Indianapolis, IN). After 24 h, cells were placed under continuous drug selection using 700 μg/ml G418 (Invitrogen, Carlsbad, CA). DBT-cACE2-His, DBT-hACE2, and DBT-GFP-His cells were passaged four times under drug selection and then sorted for high ACE2 or GFP expression levels and expanded for future use.

Cell sorting and fluorescence-activated cell sorter analysis of ACE2-expressing DBT stable cell lines. A total of 10^6 DBT (control), DBT-hACE2, and DBT-cACE2-His cells were blocked with Dulbecco's phosphate-buffered saline (DPBS)-5% fetal bovine serum and stained with polyclonal goat anti-hACE2 (R&D Systems, Minneapolis, MN), followed by a secondary anti-goat immunoglobulin G (IgG)-fluorescein isothiocyanate (FITC; Invitrogen, Carlsbad, CA) antibody. Stained DBT, DBT-hACE2, and DBT-cACE2-His and unstained DBT-GFP-His cells were sorted on a Cytomation Inc. MoFlo cell sorter (Dako, Denmark) for FITC or GFP expression, and sorted cells were expanded by four passages, after which stocks of DBT, DBT-hACE2, DBT-cACE2-His, and DBT-GFP-His cells were cryopreserved for future experiments. To assess transgene expression in postsorted cell stocks, 5×10^5 DBT, DBT-hACE2, DBT-cACE2-His, DBT-GFP-His, or Vero E6 cells were seeded into six-well dishes. Twenty-four hours later, medium was removed, and the cells were removed from the plate, with versene (UNC tissue culture facility). Cells were stained for fluorescence-activated cell sorter analysis as described above and analyzed for FITC/GFP expression by FACScan (BD Biosciences, San Jose, CA).

Western blot analysis of ACE2-expressing DBT stable cell lines. To assess transgene expression in postsorted cell stocks by Western blot analysis, DBT, DBT-hACE2, DBT-cACE2-His, DBT-GFP-His, and Vero E6 cells were seeded in six-well dishes at 5×10^5 cells/well. Twenty-four hours later, cells were lysed with protein lysis buffer (1% Triton X-100, 0.5% sodium dodecyl sulfate [SDS], in 1× Tris-buffered saline [TBS]). Twenty microliters of cell lysate was heated at 70°C in 1× NuPage buffer-4% beta-mercaptoethanol, loaded on a NuPage 12% bis-Tris SDS polyacrylamide gel (Invitrogen, Carlsbad, CA) and separated at 150 V for 2 h. Proteins were transferred to a nylon membrane, using the NuPage transfer apparatus according to the manufacturer's protocol. Membranes were blocked with 5% milk and probed with either polyclonal goat anti-human ACE2 (R&D Systems, Minneapolis, MN) or mouse anti-penta-His antibody (Qiagen, Valencia, CA). Membranes were washed with 1× TBS-0.1% Tween 20 and then probed with either rabbit anti-goat horseradish peroxidase (HRP) (Invitrogen, Carlsbad, CA) or anti-mouse IgG-HRP antibody (Amersham, Piscataway, NJ). After membranes were rinsed, they were treated with ECL Plus reagent (Amersham) and then exposed to radiographic film (Amersham).

RT-PCR to detect viral subgenomic leader-containing transcripts, ACE2, and GAPDH transcripts. RT-PCR to detect subgenomic leader-containing transcripts was performed to detect viral replication as described by Sheahan et al. (26). DBT, DBT-GFP-His, DBT-cACE2, DBT-hACE2, or Vero E6 cells were seeded at 5×10^5 cells/well in a 24-well dish. Twenty-four hours later, cells were infected with 100 μl of viral supernatant from the initial icSZ16-S transfection or icSARS virus supernatants or were mock infected. At 24 hpi, total RNA was

isolated using TRIzol reagent (Invitrogen, Carlsbad, CA) according to the manufacturer's protocol. One microgram of total RNA was used to generate cDNA by Superscript II (Invitrogen, Carlsbad, CA) using random hexamer primers (Invitrogen, Carlsbad, CA). cDNA was then used as the template for PCR using *Taq* polymerase (New England Biolabs, Ipswich, MA). Evidence of SARS-CoV replication and subgenomic mRNA 3a, E, and M (amplicon sizes, 1,796, 947, and 666 bp, respectively) was detected by using a leader forward primer (CTCTTG TAGATCTGTTCTCTAAACGAAC) and a reverse primer in the M gene (TT ACTGTACTAGCAAAGCAATATTGTCG). Detection of ACE2 transcripts was performed with a conserved primer set capable of detecting primate, human, and civet ACE2 (258 bp) (ACE2RTF2 primer, 5′-AGCCTAAAAT CAGCTCTTGG-3′; and ACE2RTR2 primer, 5′-CCGGGACATCCTGATG GC-3′). Detection of GAPDH (glyceraldehyde-3-phosphate dehydrogenase) (235 bp) (GAPDHF primer, 5′-CATGGGGAAGGTGAAGGTCG-3′; and GAPDHR primer, 5′-TTGATGGTACATGACAAGGTGC-3′) signals detected by RT-PCR was used as a positive control. PCRs were separated by gel electrophoresis on 1.8% agarose Tris-acetate-EDTA (TAE) gels and visualized by ethidium bromide staining.

Virus growth curve analysis within Vero E6, DBT-cACE2, DBT-hACE2, or DBT cells. Vero E6, DBT-cACE2, DBT-hACE2 or DBT cells were infected with the icCUHK-W1, icGD03-S, icGZ02, icSZ16-S K479N p6, icSZ16-S K479N D22, icSARS, or icSZ16-S strain, at a multiplicity of infection (MOI) of 0.01 for 1 h at 37°C, after which the inoculum was removed, the monolayer was rinsed with DPBS, and the growth medium was added. Virus stock titers generated by plaque assay in DBT-cACE2 cells were used to calculate the MOI for the DBT-cACE2 cell growth curve. Virus stock titers generated by plaque assay in Vero E6 cells were used to calculate the MOI for the Vero E6 and DBT-hACE2 growth curves. Twenty-five microliters of cell medium was removed at 0, 6, 12, 24, and 36 hpi, and samples were stored at −80°C until titers were determined by plaque assay. For all growth curves except those performed within DBT cells, the cell type used for growth curve analysis was also utilized for the titration of growth curve samples by plaque assay. For example, titers of samples generated from growth curves performed within DBT-cACE2 cells were determined with DBT-cACE2 cells. All DBT cell growth curve titers were determined with DBT-cACE2 cells. Since previous experiments suggested that Vero E6 and DBT-hACE2 cells were not permissive for icSZ16-S infection, icSZ16-S samples from DBT-hACE2 and Vero E6 growth curve titers were determined with DBT-cACE2 cells. Growth curves were performed in duplicate on two independent occasions, and the data shown are from one representative experiment.

ACE2 blockade experiments with DBT-cACE2 cells. DBT-cACE2 cells were seeded at 5×10^5 cells/well in six-well dishes. On the following day, cell medium was removed, and cells were incubated with 10, 5, 2.5, 1.25, or 0.625 μg/ml polyclonal anti-ACE2 or anti-ACE antibody (R&D Systems, Minneapolis, MN) or with DBPS for 1 h at 37°C. After the 1-h pretreatment with antibody, 100 PFU/50 μl of icSARS, icSZ16-S, or icGD03-S was added to the antibody mixture and incubated for 1 h at 37°C. After the infection, the inoculum was removed, and the monolayer was rinsed twice with 1 ml of DPBS and then overlaid with 0.9% agarose in complete growth medium. After 48 hpi, plates were stained with neutral red, and plaques were counted. The average percentage of blockade was calculated by dividing the average number of plaques per Ab dilution by the average number of plaques in the DPBS no-Ab controls. Virus stock titers generated by plaque assay in DBT-cACE2 cells were used to calculate virus concentrations for the blockade experiment. Blockade experiments were performed in duplicate on two separate occasions.

PRNT assay. Neutralizing titers were determined by plaque reduction neutralization titer (PRNT) assay as described by Rockx et al. (21, 22) and Sheahan et al. (26). Briefly, 24 h prior to infection, six-well plates were seeded with 5×10^5 DBT-cACE2 cells/well. hu-MAbs S230.15 and S3.1 directed against the SARS-CoV S protein and an isotype control antibody directed against cholera toxin D2.2 were kindly provided by A. Lanzavecchia. hu-MAbs were serially diluted twofold and incubated with 100 PFU of either icSARS, icSZ16-S, or icGD03-S for 1 h at 37°C. Virus and antibodies were then added to six-well plates of DBT-cACE2 cells in duplicate and incubated at 37°C for 1 h, after which the cells were overlaid with 0.8% agarose in medium. Plates were incubated for 48 h at 37°C and stained with neutral red for 3 h, and plaques were counted. The percentage of neutralization was calculated as 1 − (number of plaques with antibody/number of plaques without antibody) × 100%.

Computer modeling of RBD interactions with cACE2 and hACE2. Structural models for SZ16, SZ16-K479N, and SZ16 K479N D22 RBD were based on the crystal coordinates reported for SARS-CoV Urbani RBD interacting with the hACE2 receptor (Protein Data Bank [PDB] code 2AJF) as previously reported (17, 26). Using the RosettaDesign website, we incorporated the amino acid replacements, and all amino acids within the 5-Å interaction distance were relaxed to allow the program to repack the side chains to an optimal energetic state. This process was repeated with each mutation and series of mutations. Ten models were generated for each set of mutations, and the best model, based on the lowest energy score, was selected and evaluated further using Macintosh PyMOL software. In addition, the crystal structure coordinates for the SARS-CoV RBD interacting with the hACE2 receptor (PDB code 2AJF, chains A and E) were used as a template to generate a homology model for the cACE2, using Modeler software (version 8.2). Briefly, chain E of the 2AJF template was aligned to the cACE2 sequence, and five models were generated under the automodel class. The model with the lowest objective function score was selected for further analyses. The PDB files generated by this program were visualized with PyMOL for Macintosh molecular modeling (DeLano Scientific) and Chimera software.

RESULTS

Construction and characterization of ACE2-expressing stable cell lines. At the amino acid level, primate ACE2 (Vero E6) and cACE2 are 89% and 84% similar to hACE2, the human SARS-CoV receptor, respectively. In comparison to the contact interface of hACE2 with the SARS-CoV S glycoprotein, that of cACE2 differs greatly, but primate ACE2's contact interface is identical (Fig. 3E). Since previous efforts to culture either the SARS-CoV SZ16 wild type or the recombinant icSZ16-S strain were unsuccessful, we used a cell-based approach to resurrect icSZ16-S (15, 26). We constructed stable cell lines expressing cACE2-His, hACE2, and GFP-His in the DBT cell background. The gifted cACE2 gene utilized to construct our stable cells varied by two amino acids (G354D and R736Q) compared to that of the published sequence, but both G354 and D354 polymorphisms in ACE2 can be found in civet tissues (personal communication with M. Farzan) (18). Stable cells were sorted for ACE2 or GFP expression, and cultivated master cell stocks were analyzed by flow cytometry and Western blotting (Fig. 1). ACE2 expression was detected by Western blotting in cell lysates generated from DBT-hACE2, DBT-cACE2, and Vero cell cultures but was not detected in wild-type DBT cells or in DBT-GFP-His control cells (Fig. 1B). To generate quantitative data for ACE2 expression levels within our stable cells, the cell cultures were analyzed by flow cytometry. ACE2 expression in DBT-hACE2 cells appears to be greater than the expression within Vero E6 cells, while expression in DBT-cACE2 appears to be the lowest of the three ACE2-expressing cell types (Fig. 1A and C). Since the polyclonal primary antibody used to stain the cells for flow cytometry was raised against the ectodomain of hACE2, the differences we see in expression levels may be mediated by less efficient interactions between the antibody and Vero E6 ACE2 (89% amino acid homology to hACE2) or cACE2 (84% amino acid homology to hACE2) in their natural conformations. Positive control DBT-GFP-His cells exhibited a high level of GFP expression by flow cytometry and Western blot analysis. ACE2 expression was not detected in untransfected DBT cells.

Resurrection of icSZ16-S in DBT-cACE2 cells. To assess virus replication and ACE2 transgene expression in our cell panel, we employed a highly sensitive RT-PCR-based assay. In the coronavirus model of discontinuous transcription, subgenomic messages all contain the same 5′ leader sequence (24). Thus, active SARS-CoV mRNA synthesis can be detected by RT-PCR for viral subgenomic leader-containing transcripts. In our assay, we used a forward primer directed

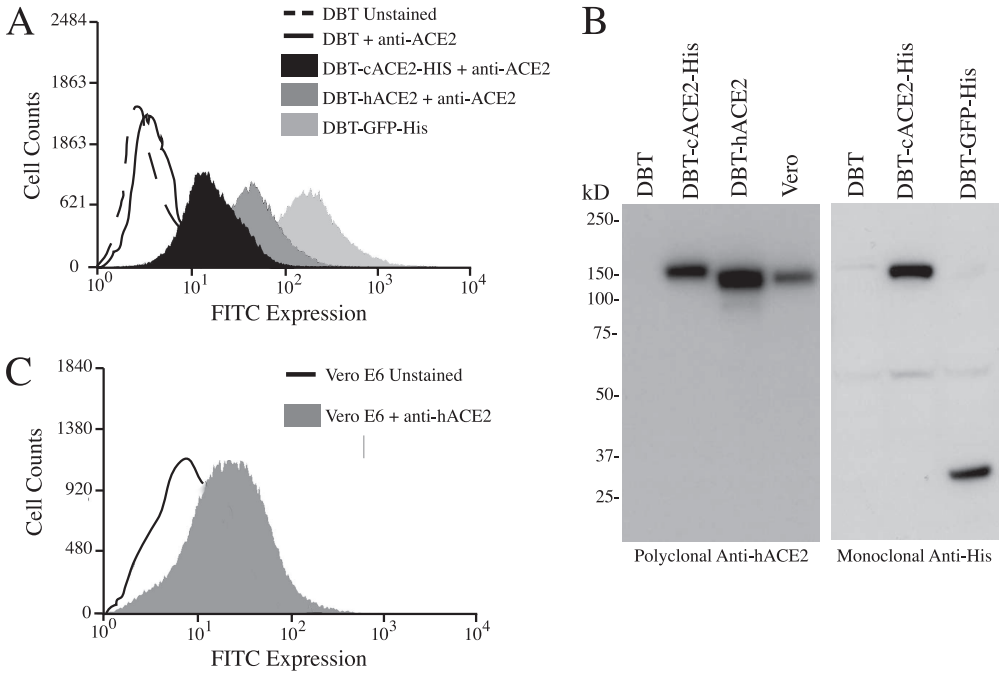

FIG. 1. Characterization of cACE2- and hACE2-expressing DBT cells by flow cytometry and Western blotting. ACE2 expression levels in Vero E6 cells or DBT cells stably expressing cACE2, hACE2, or GFP were assessed by flow cytometry and Western blotting. DBT cells stably transfected with plasmids carrying cACE2-His, hACE2, or GFP-His were passaged four times, after which cells were stained for ACE2 expression (primary antibody, polyclonal anti-hACE2; secondary antibody, anti-goat-FITC) and sorted for mid-to-high ACE2 expression (FITC). GFP control cells were also sorted for mid-to-high expression. (A and C) To assess ACE2 expression in expanded postsorted cell stocks and in Vero E6 cells, cells were stained as described above and analyzed for FITC/GFP expression by flow cytometry. (B) To assess ACE2 expression in Vero E6 cells and in postsorted cell stocks by Western blotting, similar numbers of Vero E6, DBT, DBT-hACE2, DBT-cACE2-His, and DBT-GFP-His cells were lysed and separated on a NuPage 12% bis-Tris SDS-polyacrylamide gel. After membrane transfer, blots were probed with either polyclonal goat anti-human ACE2 or mouse anti-penta-His antibody. After membranes were washed, they were probed with either rabbit anti-goat HRP or anti-mouse IgG-HRP antibody. Membranes were rinsed and treated with ECL Plus reagent and exposed to radiographic film.

against the leader sequence and a reverse primer in the M gene, allowing us to preferentially detect subgenomic transcripts encoding the open reading frame (ORF) of the 3a, E, and M genes. ACE2 transcripts were detected by RT-PCR in mock-infected cell cultures of DBT-hACE2, DBT-cACE2, and Vero E6 cells (Fig. 2A). ACE2 transcripts were not detected in DBT cells, corroborating our flow cytometry and Western blot results. As expected, GAPDH-positive control transcripts were

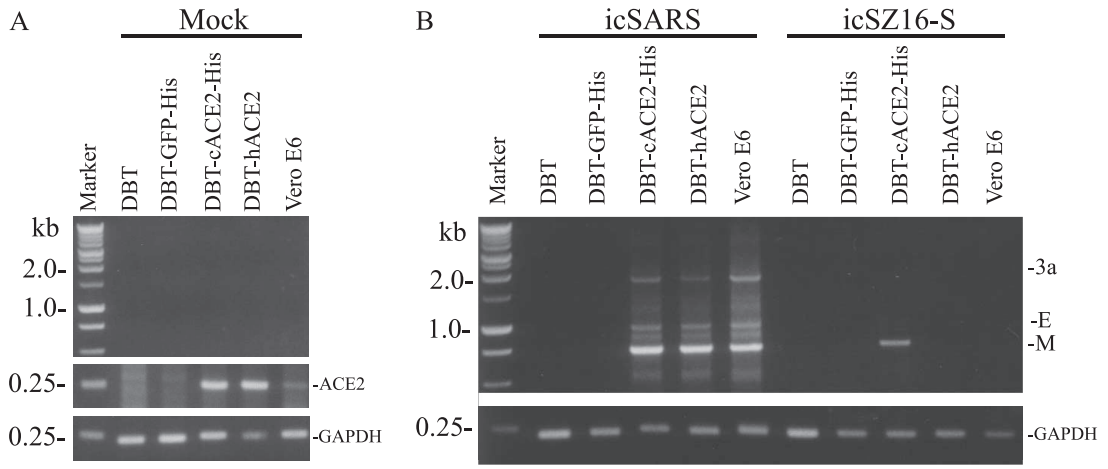

FIG. 2. Resurrection of icSZ16-S with DBT-cACE2 cells. RT-PCR to detect subgenomic leader-containing transcripts was performed to detect viral replication. DBT, DBT-GFP-His, DBT-cACE2, DBT-hACE2, or Vero E6 cells were infected with 100 μl of viral supernatant from the initial icSZ16-S transfection, or the icSARS supernatants (B), or they were mock infected (A). At 24 hpi, total RNA was isolated, and cDNA was generated and then used as template for PCR. Evidence of SARS-CoV replication and subgenomic transcription, ACE2 gene expression, and control GAPDH gene expression was detected by the production of amplicons (SARS-CoV, 3a [1,796 bp], E [947 bp], M [666 bp]; control, 235 bp GAPDH; ACE2, 258 bp) visualized by electrophoresis using a 1.8% agarose TAE gel.

detected at similar levels in all mock-infected cell cultures, while none of the mock-infected cultures was positive for SARS-CoV replication (Fig. 2A). In the icSARS virus-infected cell panel, DBT-cACE2, DBT-hACE2, and Vero E6 cells were clearly capable of supporting efficient SARS-CoV replication. Under identical conditions, SARS-CoV leader-containing transcripts were not detected in control DBT and DBT-GFP-His cells (Fig. 2B). Interestingly, only cACE2-expressing cells efficiently supported the replication of icSZ16-S (Fig. 2B). Importantly, icSZ16-S was successfully passaged and maintained in DBT-cACE2 cells in vitro, producing a robust cytopathology after four passages at 48-h intervals. Passage-four virus was plaque purified, stocks were grown, and the S, 3a, E and M genes were sequenced. Only one coding mutation (Y107H) was found in the 3a gene.

Assessment of virus growth in DBT, DBT-cACE2, DBT-hACE2, and Vero cells. Prior to this report, zoonotic SARS S virus and h/cACE2 interactions were evaluated by using pseudovirus bearing the GD03 and SZ16 S proteins, but these assays were unable to address virus growth fitness (19, 36). Moreover, one study suggested that the GD03 S protein was not dependent on ACE2 for docking and entry (36). Consequently, we assessed the growth fitness of recombinant virus bearing various S glycoproteins derived from the early, middle, and late phases of the SARS epidemic in China. We employed recombinant SARS-CoV bearing the S genes isolated from humans during the early (icGZ02), middle (icCUHK-W1), and late (icSARS) phases of the epidemic and one isolate from a sporadic human case in early 2004 (icGD03-S). The GD03, GZ02, and CUHK-W1 S glycoproteins differ from the those of the epidemic strain by 17, 8, and 2 amino acids, respectively (Fig. 3D). We also evaluated the growth of the icSZ16 parent virus and two SZ16 mutants, previously described by Sheahan et al., which were selected for efficient growth in HAE cells (26). The SZ16, SZ16-K479N, and SZ16-K479N D22 S glycoproteins differ from those of the epidemic strain by 18, 17, and 19 amino acids, respectively (26). The growth fitness of the virus panel was assessed in DBT, DBT-cACE2, DBT-hACE2, and Vero E6 cell cultures (Fig. 3A, B, and C). Cultures were infected at an MOI of 0.01 for 1 h and washed to remove input virus, and growth medium was added; then, cultures were sampled at various times postinfection. DBT cells that were not transfected with the SARS receptor ACE2 were not permissive to infection by any of the viruses tested (data not shown). In DBT-cACE2 cells, icSARS, icSZ16-S, icGZ02, and icGD03-S grew to similar peak titers by 36 hpi (Fig. 3A). In DBT-cACE2 cells at 12 hpi, the icSZ16-S titers were approximately one log higher than those of all of the other viruses tested (Fig. 3A). Interestingly, CUHK-W1 had severely delayed growth kinetics within the cACE2-expressing cells. Similarly, icSZ16-S K479N and icSZ16-S K479N D22 exhibited little to no growth in the DBT-cACE2 cells, though their S protein sequences differ from that of SZ16 by one (K479N) and three (D22) amino acids (Fig. 3A). Within DBT cells expressing hACE2, the epidemic strain exhibited superior growth fitness compared to those of the other viruses tested, with a 1 to 2 log titer advantage at 12 hpi, but icSARS, icCUHK-W1, icGZ02, icGD03-S, and icSZ16-K479N D22 grew to similar peak titers by 36 hpi. As we had seen previously, icSZ16-K479N grew poorly in the DBT-hACE2 cells, reaching titers of less than 10^4 PFU/ml, and icSZ16-S did not grow at all (Fig. 3B). Vero E6 cell growth kinetics for icSARS, icCUHK-W1, icGZ02, and icSZ16-S K479N D22 were quite similar, reaching titers of around 10^7 PFU/ml by 36 hpi, while icSZ16-S K479N and icGD03-S grew much less efficiently ($\sim 10^5$ PFU/ml at 36 hpi) (Fig. 3C). As we had seen by RT-PCR, the Vero E6 cell was not permissive to infection by icSZ16-S (Fig. 3C).

icGD03-S and icSZ16-S are dependent on ACE2 for entry. Using pseudotyped viruses, previous reports have suggested that some zoonotic SARS-CoV do not use ACE2 for entry (36). Since the SARS S pseudotyped viruses lack the other SARS-CoV structural proteins found in the SARS-CoV envelope (E, M, 3a, and 7a) and the amounts of S protein present on the surface of pseudovirus may differ from those found on the surface of a natural SARS-CoV particle, the use of SARS S pseudotyped viruses to study binding and entry might not faithfully recapitulate natural virus-cell interactions. To assess the receptor dependence of the recombinant SARS-CoV strains bearing zoonotic S proteins, we utilized a receptor antibody blockade assay (Fig. 4). Twofold dilutions of antibody (polyclonal anti-ACE2) or control antibody (polyclonal anti-ACE) were used to block ACE2 within DBT-cACE2 cells. The blocked cells were subsequently infected with 100 PFU of icSARS, icGD03-S, or icSZ16-S, rinsed and overlaid with medium containing agarose. All three viruses tested were equally dependent on ACE2 for entry, exhibiting a dose-dependent response to anti-ACE2 receptor blocking antibody (Fig. 4). Control antibody (polyclonal anti-ACE) was not capable of blocking entry of any of the viruses tested in a dose-dependent manner, firmly establishing the fact that ACE2 is a receptor for both the epidemic and the civet strains of SARS-CoV (Fig. 4).

hu-MAb S230.15 and S3.1 neutralization profiles differ between epidemic, in vitro-evolved, and zoonotic strains of SARS-CoV. hu-MAbs S230.15 and S3.1 were isolated from a convalescent SARS patient's B cells (21, 30). To assess the neutralization efficacy of these hu-MAbs, we employed a PRNT assay with the following challenge viruses: icSARS (epidemic strain S protein), icGD03-S (divergent human strain S protein), icSZ16-S (civet strain S protein), icSZ16-S K479N (SZ16 S protein mutated at residue 479 from lysine to asparagine), and icSZ16-S K479N D22 (in vitro-evolved mutant with enhanced growth in human cells whose S protein is mutated at Y442F and L472F). The broadly neutralizing hu-MAb S230.15 was able to neutralize 50% ($PRNT_{50}$) of icSARS virus and the evolved icSZ16-S K479N D22 virus, using less than 0.03125 μg/ml of antibody, while icGD03-S, icSZ16-S K479N and icSZ16-S were approximately four times more resistant ($PRNT_{50}$ = 0.125 μg/ml) (Fig. 5A). The S3.1 hu-MAb was not as effective at neutralizing the viruses tested ($PRNT_{50}$ for icSARS and icSZ16-S K479N was 0.25 μg/ml and for icSZ16-S K479N D22 was 0.625 μg/ml) (Fig. 5B). Unlike hu-MAb S230.15, hu-MAb S3.1 was weakly efficacious against icGD03-S ($PRNT_{50} > 1$ μg/ml) and completely ineffective against icSZ16-S (Fig. 5B).

Structural models of SARS and ACE2 interactions. To gain a better understanding of the structural changes associated with the mutation of both the S and the ACE2 proteins, we developed predictive structural models of S and cACE2/hACE2 interactions using RosettaDesign and Modeler software. Our models suggest that additional methyl groups in E30 and Y34 of cACE2 likely

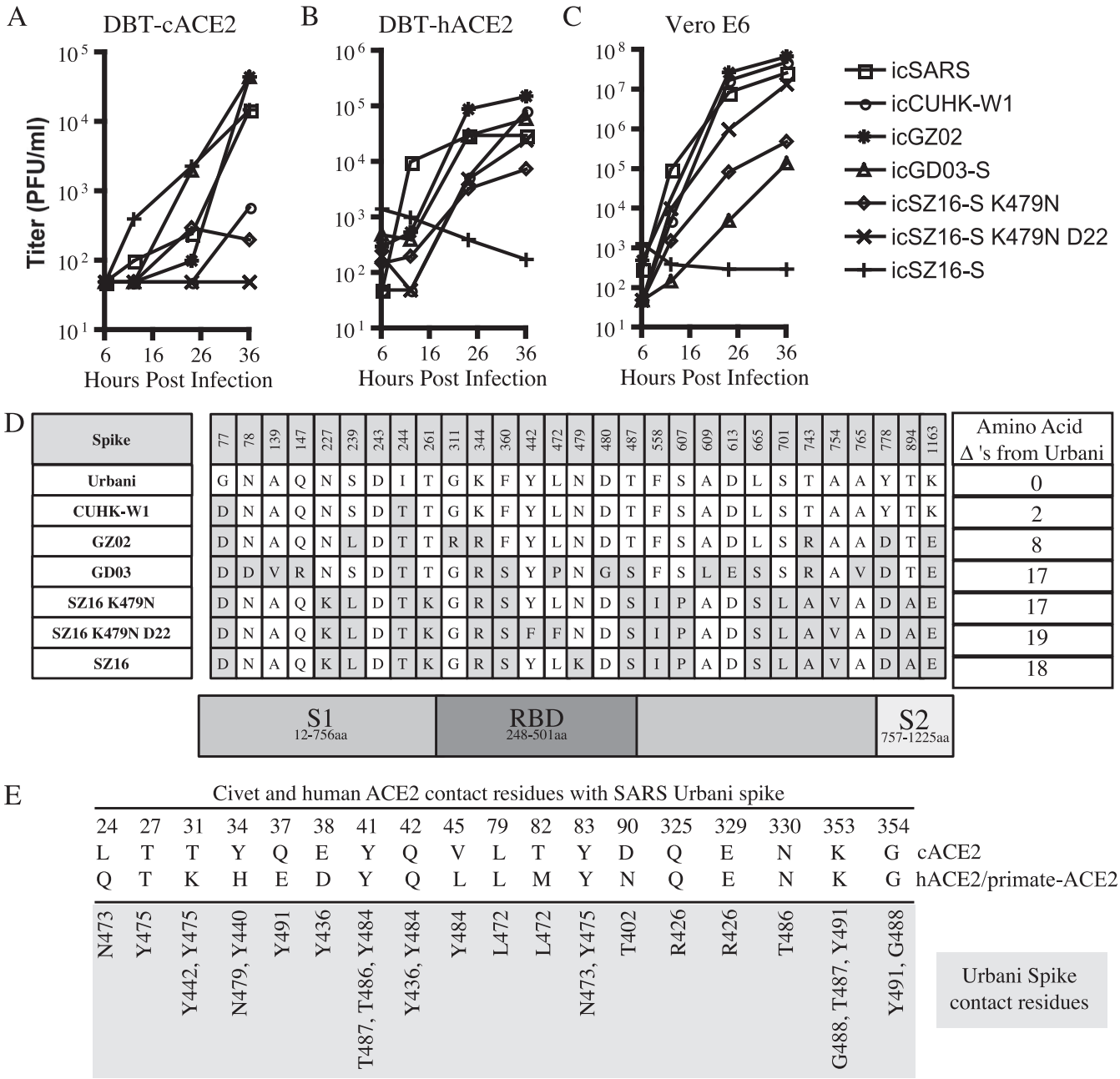

FIG. 3. Assessment of virus growth in DBT, DBT-cACE2, DBT-hACE2, and Vero cells, the spike amino acid variation in our recombinant virus panel, and the ACE2 contact residues with the Urbani spike. DBT-cACE2 (A), DBT-hACE2 (B), Vero E6 (C), or DBT (data not shown) cells were infected with icCUHK-W1, icGD03-S, icGZ02, icSZ16-S K479N p6, icSZ16-S K479N D22, icSARS, or icSZ16-S at an MOI of 0.01 for 1 h at 37°C. Cell medium (25 μl) was removed at 0, 6, 12, 24, and 36 hpi, and samples were stored at −80°C until titers were determine by plaque assay. Growth curves were performed in duplicate on two separate occasions, and the data shown are representative of one experiment. (D) The location of spike amino acid differences among the recombinant virus panels. (E) Urbani, cACE2, primate-ACE2, and hACE2 contact residues, adapted from the crystal structure published by Li et al. (17).

create a protrusion from the binding interface that is enhanced compared to that of hACE2. The architecture of the Urbani RBD can accommodate this protrusion on the cACE2 binding interface, thus retaining efficient binding to both cACE2 and hACE2 (Fig. 6A and B). We and others have previously published structural models that suggest that K479 of the SZ16 S protein inhibits binding to hACE2 because of electrostatic clashes with the hACE2 binding partners K31 and H34, but the SZ16 binding partners within cACE2 are different (Y34 and E30) and allow for efficient binding of SZ16 S (Fig. 6C) (17, 19, 26). Interestingly, the human ACE2 adaptive mutations in SZ16 K479N and SZ16 K479N D22 that progressively remodel the RBD binding interface to enhance binding to hACE2 (Fig. 6D and F) create a steric clash between the RBDs V404/Y440 and E30/Y34 of cACE2

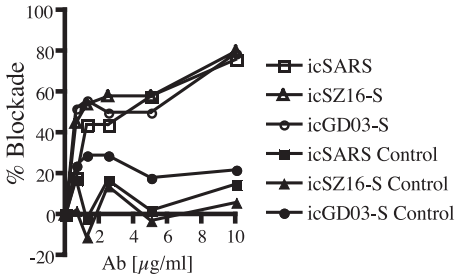

FIG. 4. icGD03-S and icSZ16-S are dependent on ACE2 for entry. DBT-cACE2 cells were seeded at 5×10^5 cells/well in six-well dishes. The following day, cell medium was removed, and cells were incubated with 10, 5, 2.5, 1.25, or 0.625 μg/ml polyclonal anti-ACE2 or anti-ACE or DBPS for 1 h at 37°C. After the 1-h pretreatment with antibody, 100 PFU/50 μl of icSARS, icSZ16-S, or icGD03-S was added to the monolayer and incubated for 1 h at 37°C. After the infection, the inoculum was removed and the monolayer was rinsed with DPBS and then overlaid with 0.9% agarose in complete growth medium. At 48 hpi, plates were stained with neutral red, and plaques were counted. The average percentage of blockade was calculated by dividing the average number of plaques per Ab dilution by the average number of plaques in the DPBS no-Ab controls. Blockade experiments were performed in duplicate on two separate occasions.

(Fig. 6E and G). Similar to that which we had seen with in vitro growth analysis, the SZ16 K479N and D22 binding interfaces cannot accommodate the enhanced protrusion of cACE2 and are unable to bind efficiently.

DISCUSSION

The recent emergence of viruses like SARS-CoV, Ebola, influenza H5N1, Marburg, and Nipah virus highlights the pathogenic and epidemic potential of zoonoses in human populations (7, 10, 16, 29, 32). The identification of zoonotic virus animal reservoirs is often unsuccessful, hampering our ability to understand the epidemiology of zoonotic diseases and the conditions required for zoonotic host range expansion. Extensive virus sequencing efforts allowed the identification of palm civets as a potential amplification host for SARS-CoV and Chinese horseshoe bats as the potential SARS-CoV animal reservoir within a short span of 2 years (2, 8). Though sequencing efforts have revealed much about the biology of zoonotic SARS-CoV, bat and civet isolates have not yet been cultured in vitro (13, 15). Using synthetic biology and reverse genetics, we constructed a SARS-CoV bearing a civet SZ16 S glycoprotein. In corroboration with Lau and Peiris, we have shown that icSZ16-S could not be maintained by passage in cell cultures that normally support SARS-CoV infection (15). Without the successful cultivation of zoonotic SARS-CoV, their mechanisms of host range expansion and pathogenic potential remain elusive, and the efficacy of current therapies against zoonotic strains remains unknown.

Rather than mutate the SZ16 S glycoprotein to promote growth in cell culture, we constructed a stable cell line expressing the cACE2 orthologue of the human SARS-CoV receptor (hACE2). Compared to the published gene sequence, the cACE2 gene utilized to construct our stable cells differed by two residues, G354D and R736Q, but only the residue G354 resides at a proposed interaction site with the SARS S RBD (Y491 and G488) (17). Residue 354 is polymorphic in nature, where some civet samples contain the G354 ACE2 mutation, while others contain the D354 ACE2 mutation (personal communication, M. Farzan) (18). All of the viruses used within this study have the same amino acid at residues 491 (tyrosine) and 488 (glycine) (Fig. 3E). In turn, if the G354D mutation in our cACE2 protein has a deleterious effect on binding and entry, we predict that all viruses would be affected equally. As our data regarding Urbani and SZ16 binding to cACE2 and hACE2 are concordant with previously published data by Li et al., it is unlikely that the G354D mutation in cACE2 is altering our virus growth phenotypes, and this hypothesis is supported by our predictive structural modeling which suggests that the G354D mutation does not affect the conformation of the cACE2 binding interface (data not shown) (19).

Using DBT-cACE2 cells, we have demonstrated that icSZ16-S can be grown, maintained, and plaque purified. In support of Li et al., we have shown that civet SARS-CoV utilizes cACE2 but cannot utilize hACE2 or Vero E6 ACE2,

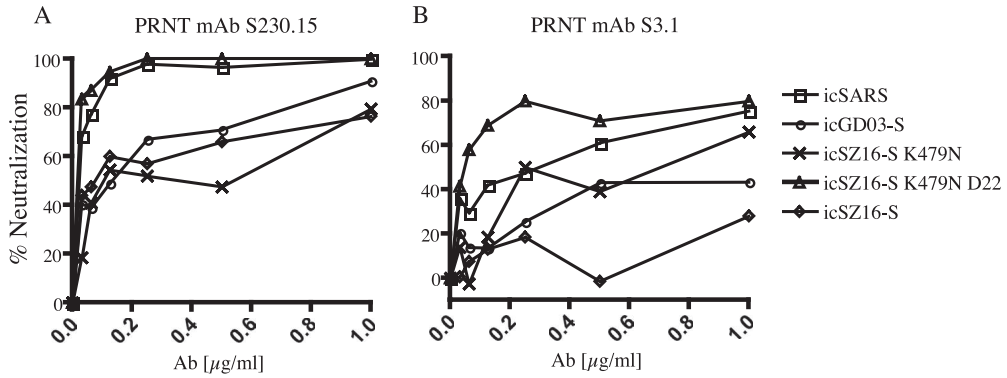

FIG. 5. hu-MAb S230.15 and S3.1 neutralization profiles differ between the epidemic, the in vitro-evolved, and the zoonotic strains of SARS-CoV. Neutralizing titers were determined by PRNT assay. Twenty-four hours before cells were infected, six-well plates were seeded with 5×10^5 DBT-cACE2 cells/well. hu-MAb S230.15 and S3.1 and an isotype control antibody directed against cholera toxin, D2.2, were serially diluted twofold and incubated with 100 PFU of either icSARS, icSZ16-S, or icGD03-S for 1 h at 37°C. Virus and antibodies were then added to six-well plates of DBT-cACE2 cells in duplicate and incubated at 37°C for 1 h, after which the cells were overlaid with 3 ml of 0.8% agarose in medium. After 48 h, plates were stained with neutral red, and plaques were counted. The percentage of neutralization was calculated as 1 − (number of plaques with antibody/number of plaques without antibody) × 100%.

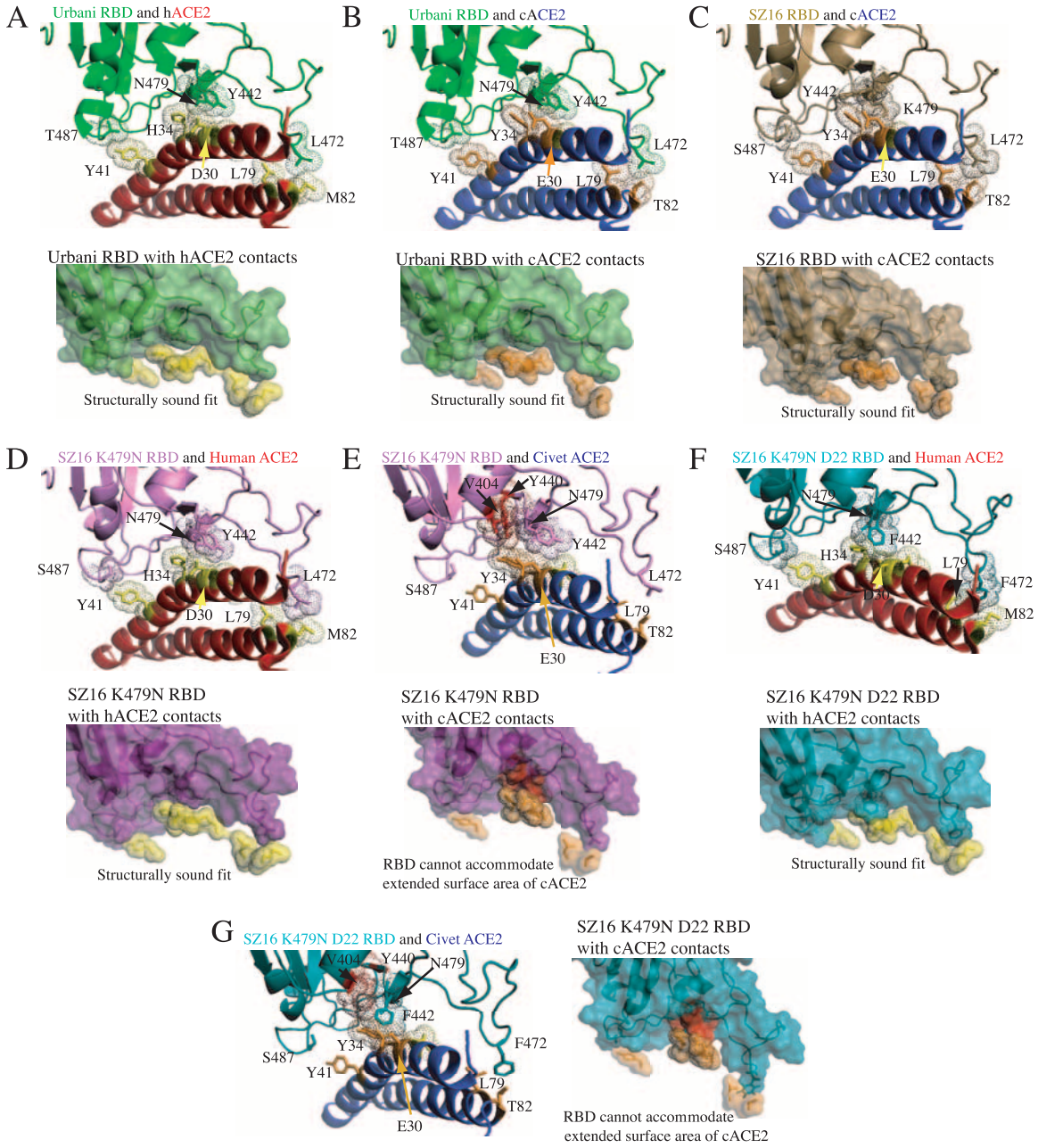

FIG. 6. Molecular modeling demonstrating structural mechanisms of ACE2 tropism. Based on the reported crystal coordinates of SARS Urbani RBD interacting with the hACE2 receptor, we generated models of Urbani, SZ16, SZ16-K479N, and SZ16 K479N D22 RBD interactions with either cACE2 or hACE2, using RosettaDesign and Modeler software. Ribbon structures and "space filling" schematics of each RBD and ACE2 combination are shown. Dotted spheres around the RBD and ACE2 residues indicate they are within 4 Å and thus are predicted to interact. Red spheres around the RBD and ACE2 residues indicate a steric clash. (A) Urbani RBD and hACE2 architecture. (B) Additional methyl groups of the cACE2 E30 and Y34 mutations add a surface protrusion to the contact interface. The Urbani RBD can accommodate the increased surface protrusion of cACE2, thereby retaining an efficient binding interface. (C) Similar to the Urbani RBD, the SZ16 RBD can accommodate the increased surface protrusion of cACE2 for efficient binding. (D) The N479 mutation in SZ16 K479N remodels the SZ16 binding interface to promote binding to hACE2. (E) The remodeling of the SZ16 K479N binding interface by the N479 mutation creates a clash between S residues (V404 and Y440) and cACE2 residues (E30 and Y34), blocking S and ACE2 binding. The SZ16 K479N RBD cannot accommodate the extended surface protrusion of the cACE2 RBD. (F) In addition to the N479 mutation, the F442 and F472 mutations further remodel the SZ16 K479N D22 RBD, further enhancing the binding efficiency to hACE2. (G) Similar to the SZ16 K479N RBD interaction with cACE2, the interaction of the SZ16 K479N D22 RBD cannot accommodate the protrusion of cACE2, abrogating binding.

confirming that the civet SZ16 virus is restricted in its host range (Fig. 2B). Using pseudotyped lentivirus, Li et al. showed that the SARS Urbani S protein was capable of utilizing both cACE2 and hACE2, and we confirmed these data by showing that icSARS is capable of infecting both cACE2- and hACE2-expressing cells and replicating to a high titer (Fig. 2B and 3A and B). In support of our RT-PCR data suggesting that icSZ16-S was restricted in its host range (Fig. 2B), icSZ16-S

grew only within cACE2-expressing cells and grew to titers similar to those of the epidemic strains icGD03-S and icGZ02 (Fig. 3 A, B, and C). Interestingly, icSZ16-S exhibited a clear growth advantage at 12 hpi, suggesting that it might gain entry into cACE2-expressing cells more rapidly than the other viruses tested. The icSZ16-S K479N and D22 viruses were adapted for efficient growth on a primary HAE cell culture, which is known to be a robust and relevant model of the complex human airway epithelium (27). Importantly, these viruses did not grow efficiently within DBT-cACE2 cells, suggesting that HAE cell growth-enhancing mutations in the civet S (K479N, Y442F and L472F) proteins diminished binding of the icSZ16-S K479N/D22 S protein to cACE2. To conclusively demonstrate that differences in the cACE2 binding affinities of the icSZ16-S, icSZ16-S K479N, and D22 viruses account for the observed differences in growth kinetics, binding and entry assays will be performed in the future. In hACE2-expressing cells, the epidemic strain displayed a clear growth advantage at 12 hpi, but most all of the viruses tested grew to similar peak titers by 36 hpi. In Vero E6 cells, the viruses bearing S proteins that were more similar to that of the epidemic strain (CUHK-W1, GZ02) grew to peak titers that were far greater than those of viruses bearing the S proteins that were more civet-like (SZ16, GD03, and SZ16 K479N). As we had expected, icSZ16-S was not capable of growth within DBT-hACE2 or Vero E6 cells, but mutations in the SZ16 S protein at select interaction sites with ACE2 (K479N, Y442F, L472F) rescued and promoted growth in hACE2 or Vero E6 cells. These data suggest that the SARS-CoV S and receptor interactions are quite specific and capable of restricting the host range or limiting infection efficiency. Moreover, these data also suggest that very few mutations in the civet S protein can enhance infection of human cells (K479N, Y442F, L472F) and simultaneously abrogate infection of cACE2-expressing cells. A corollary is seen in the more human-tropic strains. icCUHK-W1, a middle-phase epidemic isolate whose S protein differs from that of Urbani by two amino acids, is quite capable of infecting cells expressing hACE2 while it grows very poorly in cACE2-expressing cells compared to the epidemic strain. These data suggest that G77 and/or I244 of the epidemic strain enhances growth in cACE2-expressing cells. Though G77 and I244 reside outside of the RBD (amino acids 248 to 501), their close proximity to the RBD may either promote a conformational rearrangement of the S protein, subtly altering the S binding interface through long-range protein interactions, or somehow contribute to binding or entry by an unknown mechanism. Through the passage of zoonotic S-bearing SARS-CoV on Vero E6 cells, Rockx et al. described mutations just outside of the RBD (HC/SZ/61/03; amino acid positions 578; and A031G, amino acid position 577) that seemed to enhance growth, suggesting that mutations outside of the RBD may influence the architecture of the binding interface or enhance binding and entry by an unknown mechanism (22). All together, the growth curve data highlight the plasticity of both zoonotic and human-tropic SARS-CoV S proteins, where the subtle remodeling RBD can both enhance and abrogate binding to ACE2.

Serological evaluation of workers in wet markets suggests that zoonotic SARS-CoV was transmitted to humans, though these seropositive individuals did not present clinically with SARS (1). These data support the hypothesis that repeated transfer of zoonotic SARS-CoV from civet to human and/or from human to civet fostered the evolution of the epidemic strain. Alternatively, repeated single introductions of civet SARS-CoV into the human population may eventually have resulted in the generation of a human-tropic SARS-CoV that coincidently retained affinity for cACE2. Our growth curve analyses demonstrating that the epidemic strain is equally fit at growth within cACE2- or hACE2-expressing cells supports both evolutionary hypotheses. In fact, recent data suggest that civets infected with human-tropic SARS-CoV develop symptoms and a pathology similar to those seen in human cases of SARS-CoV infection (35). Our predictive RBD and ACE2 structure model data provide a possible explanation of how the dual host tropism of SARS Urbani is retained. The cACE2 molecule differs from that of hACE2 by two key residues (E30 and Y34), which likely creates a pronounced protrusion from the cACE2 binding interface. The Urbani RBD is able to accommodate the various binding interfaces of both cACE2 and hACE2, thus retaining dual host tropism. We also demonstrate that the SZ16 lineage viruses passaged with HAE cells, in the absence of cACE2, evolved a mutant RBD that allowed for more efficient binding of hACE2 (icSZ16-S K479N, D22) but simultaneously lost the ability to efficiently infect cACE2-expressing cells. Our predictive structural models suggest that the human adaptive RBD mutations in icSZ16-S K479N and D22 abrogate their abilities to accommodate the protrusive cACE2 binding interfaces. Therefore, we hypothesize that in the absence of evolutionary pressure to retain the ability to grow within both cACE2- and hACE2-expressing cells, a series of mutations are acquired to enhance binding to only one of the two receptors. We might have been able to generate a strain more similar to the dual tropic epidemic strain had we done repeated passages of the icSZ16-S virus, alternating between cACE2- and hACE2-expressing cells. Nevertheless, these data suggest that the natural evolution of the epidemic strain probably occurred through repeated transfer of virus from civet to human and from human to civet over a long period of time, providing the evolutionary pressure to retain dual ACE2 tropism. This hypothesis is supported by three serological surveys performed to determine the prevalence of SARS-CoV-specific IgG in healthy subjects in China. First, samples collected from volunteers in Guangdong province in China, in May 2003, demonstrated that SARS virus-specific IgG was found in animal traders (13%; $n = 508$), hospital workers (2.9%; $n = 137$), Guangdong CDC workers (1.6%; $n = 63$), and healthy adults at the clinic (1.2%; $n = 84$) (1). The second study was a retrospective serological survey performed with 1,621 serum samples from March 2002, isolated from healthy 18-year-old male Chinese soldiers from 17 provinces, including Guangdong (39). Of these 1,621 samples, 0.68% tested positive for SARS-CoV by enzyme-linked immunosorbent assay, though the provinces that the SARS-CoV IgG-positive soldiers inhabited were not mentioned. A third study retrospectively examined 938 serum samples collected in May of 2001 from healthy adults in Hong Kong. Shockingly, 1.8% of these samples collected 2 years prior to the epidemic tested positive for SARS-CoV by immunofluorescence assay (40). These data suggest that less serious or asymptomatic cases of SARS-CoV existed at least 2 years prior to the beginning of the epidemic in various geographical locations in

China. If the populations sampled in the May 2003 cohort are representative of the Guangdong province population (estimated population of 100,000,000), there were probably many more unreported or less serious cases (>1,000,000) of SARS-CoV infection prior to the evolution of the highly pathogenic epidemic strain of 2002 to 2003.

Though molecular evolution studies of SARS-CoV genomes have demonstrated that the S gene had undergone a significant amount of mutation and positive selection during the early phases of the epidemic, the nonstructural ORF1a demonstrated a similar pattern (2). We have chosen to focus on the importance of the S mutation and ACE2 interaction for viral evolution and host range expansion, but the molecular genetic data clearly suggest that mutation of nonstructural genes may also have been important for the efficient adaptation to new hosts.

In 2005, Yang et al. reported that pseudoviruses bearing the zoonotic S (GD03 and SZ3) protein were much less dependent on ACE2 for entry in 786-O cells (36). Using 786-O cells and similar pseudoviruses bearing the Tor2, GD03, or SZ3 S proteins, both Li et al. and He et al. were not able to infect 786-O cells with pseudoviruses (9, 19). Since SARS S pseudotyped viruses lack SARS-CoV membrane-bound proteins (E, M, 3a, 7a) and may contain unnatural amounts of surface SARS S glycoprotein, pseudovirus may produce false-positive or false-negative results for binding and entry assays. Moreover, the pseudovirus systems are limited to the evaluation of binding and entry and are unable to evaluate the effects of zoonotic glycoproteins on replication and growth. To reevaluate the pseudovirus findings in the context of natural SARS-CoV infection, we constructed SARS-CoV strains bearing zoonotic S proteins. The SZ3 S protein differs from that of SZ16 by one amino acid outside of the RBD (SZ3 F558, SZ16 I558). Since our molecular and growth curve data suggested that icSZ16-S efficiently infects only cACE2-expressing cells, we performed receptor blockade experiments with DBT-cACE2 cells. We found that icSARS, icSZ16-S, and icGD03-S were similarly blocked from entry in a dose-dependent manner, using an antibody directed against ACE2, while the control antibody had little effect. Though we did not achieve 100% blockade with the highest concentration of antibody tested, we believe that polyclonal anti-hACE2 may interact less efficiently with native cACE2. Alternatively, we may not have completely saturated the available surface cACE2, which would result in an incomplete blockade. At this time, we believe it is more likely that our inability to block 100% of infection was due the technical issues discussed above and less likely that zoonotic viruses gain entry into cells via alternative receptors. Since the viruses we evaluated could not productively infect nontransfected DBT cells, it is unlikely that the incomplete block in entry with the Ab was due to entry via alternative receptors. However, coreceptors (L-SIGN) have been reported for SARS-CoV, but to our knowledge, the ability of zoonotic SARS-CoV to engage these receptors has not been rigorously examined (11). Therefore, we believe we most likely did not block 20% of the surface ACE2 with 10 μg/ml Ab.

Since it is impossible to predict the antigenic identity of future emergent SARS viruses, the development of highly cross-reactive antibody, drug, or vaccination therapies would provide the greatest potential benefit to public health. Recently, we and others have shown that hu-MAb S230.15 was less effective at neutralizing icSZ16-S K479N in vitro but was very effective in passive transfer studies with mice, lowering viral titers of both icGD03-S and icSZ16-S K479N below the detectable limit (41). In in vitro PRNT assays, icSZ16-S and icGD03-S were also more resistant to neutralization by S230.15 than the epidemic strain. Since icSZ16-S and icGD03-S are similarly neutralized by S230.15 in vitro, passive transfer studies by Zhu et al. suggest that S230.15 would be effective against icSZ16-S in vivo as well (41). Yang et al. described an antibody-dependent enhancement phenomenon using hu-MAb S3.1 in neutralization assays with 786-O cells, using the GD03 and SZ16 pseudoviruses (36). We performed PRNT assays with cACE2 cells, using icSARS, icSZ16-S, and icGD03-S, and found that S3.1 is moderately effective against icSARS, weakly effective against icGD03-S, and ineffective against icSZ16-S. Since there was such a dynamic range of neutralization efficacies using S3.1 against a panel of epidemic and zoonotic SARS-CoV, these data highlight the pitfalls of using only the epidemic strain when passive immunization or vaccination therapies are evaluated. Of note, ter Meulen et al. explored the possibility of antibody-dependent enhancement in human macrophages using SARS-CoV and subneutralizing concentrations of monoclonal antibodies and found that SARS-CoV is taken up by macrophages but does not productively infect the cells (28).

Coronaviruses similar to SARS Urbani are currently circulating within bat species in China. Constant surveillance and biological evaluation of zoonotic pools of coronavirus are impractical, making it quite difficult to predict the antigenic identity of emergent SARS-CoV-like viruses in the future. Therefore, it is imperative that current antiviral therapies be broadly cross-reactive against all known SARS-CoV, thereby maximizing the potential public health benefit. We have constructed a SARS-CoV bearing the prototypic civet S protein from the SZ16 strain. Prior to this publication, SARS-CoVs bearing the SZ16 S protein were not able to be propagated in vitro, hampering the study of the SZ16 biology and its pathogenic potential. We have demonstrated that icSZ16-S can be propagated in vitro in DBT-cACE2 cell cultures, that it is dependent on ACE2 for entry, and that it is incapable of using hACE2 for entry. We have also demonstrated that point mutations in the SZ16 S protein that enhance virus growth in primary HAE or DBT-hACE2 cells severely diminish growth in DBT-cACE2 cells, while the epidemic strain retains dual ACE2 tropism. These data and retrospective serological surveys in China suggest that the natural evolution of the epidemic strain probably occurred over a long period of time through the repeated transfer of virus from civet to human and from human to civet and that this dual host evolutionary scenario provided the evolutionary pressure to retain dual ACE2 tropism. We have also demonstrated that both icGD03-S and icSZ16-S are neutralized by hu-MAb S230.15 but are more resistant to S3.1, highlighting the utility of using an antigenically diverse SARS-CoV panel to assess serotherapy efficacy. The icSZ16-S virus is yet another antigenically divergent zoonotic S protein-bearing SARS-CoV that will prove useful in evaluating future serotherapies or vaccination therapies.

ACKNOWLEDGMENTS

We thank Michael Farzan, Harvard Medical School, Boston, MA, for kindly providing the cACE2 and hACE2 expression plasmids. We also thank Antonio Lanzevecchia, Institute for Research in Biomedicine, Bellinzona, Switzerland, for graciously providing hu-MAbs S230.15, S3.1, and D2.2. We also thank Amy Sims and Boyd Yount for world-class technical assistance and superb cloning advice.

This work was supported by research grants (R01 AI059136 and AI059443) to R.B. from the National Institutes of Health, Division of Allergy and Infectious Diseases.

REFERENCES

1. **Centers for Disease Control and Prevention.** 2003. Prevalence of IgG antibody to SARS-associated coronavirus in animal traders—Guangdong Province, China, 2003. MMWR Morb. Mortal. Wkly. Rep. **52:**986–987.
2. **Chinese SARS Molecular Epidemiology Consortium.** 2004. Molecular evolution of the SARS coronavirus during the course of the SARS epidemic in China. Science **303:**1666–1669.
3. **Christian, M. D., S. M. Poutanen, M. R. Loutfy, M. P. Muller, and D. E. Low.** 2004. Severe acute respiratory syndrome. Clin. Infect. Dis. **38:**1420–1427.
4. **Deming, D., T. Sheahan, M. Heise, B. Yount, N. Davis, A. Sims, M. Suthar, J. Harkema, A. Whitmore, R. Pickles, A. West, E. Donaldson, K. Curtis, R. Johnston, and R. Baric.** 2006. Vaccine efficacy in senescent mice challenged with recombinant SARS-CoV bearing epidemic and zoonotic spike variants. PLoS Med. **3:**e525.
5. **Dominguez, S. R., T. J. O'Shea, L. M. Oko, and K. V. Holmes.** 2007. Detection of group 1 coronaviruses in bats in North America. Emerg Infect. Dis. **13:**1295–1300.
6. **Dong, B. Q., W. Liu, X. H. Fan, D. Vijaykrishna, X. C. Tang, F. Gao, L. F. Li, G. J. Li, J. X. Zhang, L. Q. Yang, L. L. Poon, S. Y. Zhang, J. S. Peiris, G. J. Smith, H. Chen, and Y. Guan.** 2007. Detection of a novel and highly divergent coronavirus from Asian leopard cats and Chinese ferret badgers in Southern China. J. Virol. **81:**6920–6926.
7. **Gonzalez, J. P., X. Pourrut, and E. Leroy.** 2007. Ebola virus and other filoviruses. Curr. Top. Microbiol. Immunol. **315:**363–387.
8. **Guan, Y., B. J. Zheng, Y. Q. He, X. L. Liu, Z. X. Zhuang, C. L. Cheung, S. W. Luo, P. H. Li, L. J. Zhang, Y. J. Guan, K. M. Butt, K. L. Wong, K. W. Chan, W. Lim, K. F. Shortridge, K. Y. Yuen, J. S. Peiris, and L. L. Poon.** 2003. Isolation and characterization of viruses related to the SARS coronavirus from animals in southern China. Science **302:**276–278.
9. **He, Y., J. Li, W. Li, S. Lustigman, M. Farzan, and S. Jiang.** 2006. Cross-neutralization of human and palm civet severe acute respiratory syndrome coronaviruses by antibodies targeting the receptor-binding domain of spike protein. J. Immunol. **176:**6085–6092.
10. **Hsu, V. P., M. J. Hossain, U. D. Parashar, M. M. Ali, T. G. Ksiazek, I. Kuzmin, M. Niezgoda, C. Rupprecht, J. Bresee, and R. F. Breiman.** 2004. Nipah virus encephalitis reemergence, Bangladesh. Emerg. Infect. Dis. **10:**2082–2087.
11. **Jeffers, S. A., S. M. Tusell, L. Gillim-Ross, E. M. Hemmila, J. E. Achenbach, G. J. Babcock, W. D. Thomas, Jr., L. B. Thackray, M. D. Young, R. J. Mason, D. M. Ambrosino, D. E. Wentworth, J. C. Demartini, and K. V. Holmes.** 2004. CD209L (L-SIGN) is a receptor for severe acute respiratory syndrome coronavirus. Proc. Natl. Acad. Sci. USA **101:**15748–15753.
12. **Kan, B., M. Wang, H. Jing, H. Xu, X. Jiang, M. Yan, W. Liang, H. Zheng, K. Wan, Q. Liu, B. Cui, Y. Xu, E. Zhang, H. Wang, J. Ye, G. Li, M. Li, Z. Cui, X. Qi, K. Chen, L. Du, K. Gao, Y. T. Zhao, X. Z. Zou, Y. J. Feng, Y. F. Gao, R. Hai, D. Yu, Y. Guan, and J. Xu.** 2005. Molecular evolution analysis and geographic investigation of severe acute respiratory syndrome coronavirus-like virus in palm civets at an animal market and on farms. J. Virol. **79:**11892–11900.
13. **Lau, S. K., P. C. Woo, K. S. Li, Y. Huang, H. W. Tsoi, B. H. Wong, S. S. Wong, S. Y. Leung, K. H. Chan, and K. Y. Yuen.** 2005. Severe acute respiratory syndrome coronavirus-like virus in Chinese horseshoe bats. Proc. Natl. Acad. Sci. USA **102:**14040–14045.
14. **Lau, S. K., P. C. Woo, K. S. Li, Y. Huang, M. Wang, C. S. Lam, H. Xu, R. Guo, K. H. Chan, B. J. Zheng, and K. Y. Yuen.** 2007. Complete genome sequence of bat coronavirus HKU2 from Chinese horseshoe bats revealed a much smaller spike gene with a different evolutionary lineage from the rest of the genome. Virology **367:**428–439.
15. **Lau, Y. L., and J. S. Peiris.** 2005. Pathogenesis of severe acute respiratory syndrome. Curr. Opin. Immunol. **17:**404–410.
16. **Leroy, E. M., B. Kumulungui, X. Pourrut, P. Rouquet, A. Hassanin, P. Yaba, A. Delicat, J. T. Paweska, J. P. Gonzalez, and R. Swanepoel.** 2005. Fruit bats as reservoirs of Ebola virus. Nature **438:**575–576.
17. **Li, F., W. Li, M. Farzan, and S. C. Harrison.** 2005. Structure of SARS coronavirus spike receptor-binding domain complexed with receptor. Science **309:**1864–1868.
18. **Li, W., J. Sui, I. C. Huang, J. H. Kuhn, S. R. Radoshitzky, W. A. Marasco, H. Choe, and M. Farzan.** 2007. The S proteins of human coronavirus NL63 and severe acute respiratory syndrome coronavirus bind overlapping regions of ACE2. Virology **367:**367–374.
19. **Li, W., C. Zhang, J. Sui, J. H. Kuhn, M. J. Moore, S. Luo, S. K. Wong, I. C. Huang, K. Xu, N. Vasilieva, A. Murakami, Y. He, W. A. Marasco, Y. Guan, H. Choe, and M. Farzan.** 2005. Receptor and viral determinants of SARS-coronavirus adaptation to human ACE2. EMBO J. **24:**1634–1643.
20. **Muller, M. A., J. T. Paweska, P. A. Leman, C. Drosten, K. Grywna, A. Kemp, L. Braack, K. Sonnenberg, M. Niedrig, and R. Swanepoel.** 2007. Coronavirus antibodies in African bat species. Emerg. Infect. Dis. **13:**1367–1370.
21. **Rockx, B., D. Corti, E. Donaldson, T. Sheahan, K. Stadler, A. Lanzavecchia, and R. Baric.** 2008. Structural basis for potent cross-neutralizing human monoclonal antibody protection against lethal human and zoonotic SARS-CoV challenge. J. Virol. **82:**3220–3235.
22. **Rockx, B., T. Sheahan, E. Donaldson, J. Harkema, A. Sims, M. Heise, R. Pickles, M. Cameron, D. Kelvin, and R. Baric.** 2007. Synthetic reconstruction of zoonotic and early human severe acute respiratory syndrome coronavirus isolates that produce fatal disease in aged mice. J. Virol. **81:**7410–7423.
23. **Rota, P. A., M. S. Oberste, S. S. Monroe, W. A. Nix, R. Campagnoli, J. P. Icenogle, S. Penaranda, B. Bankamp, K. Maher, M. H. Chen, S. Tong, A. Tamin, L. Lowe, M. Frace, J. L. DeRisi, Q. Chen, D. Wang, D. D. Erdman, T. C. Peret, C. Burns, T. G. Ksiazek, P. E. Rollin, A. Sanchez, S. Liffick, B. Holloway, J. Limor, K. McCaustland, M. Olsen-Rasmussen, R. Fouchier, S. Gunther, A. D. Osterhaus, C. Drosten, M. A. Pallansch, L. J. Anderson, and W. J. Bellini.** 2003. Characterization of a novel coronavirus associated with severe acute respiratory syndrome. Science **300:**1394–1399.
24. **Sawicki, S. G., D. L. Sawicki, and S. G. Siddell.** 2007. A contemporary view of coronavirus transcription. J. Virol. **81:**20–29.
25. **Sheahan, T., D. Deming, E. Donaldson, R. Pickles, and R. Baric.** 2006. Resurrection of an "extinct" SARS-CoV isolate GD03 from late 2003. Adv. Exp. Med. Biol. **581:**547–550.
26. **Sheahan, T., B. Rockx, E. Donaldson, A. Sims, R. Pickles, D. Corti, and R. Baric.** 2008. Mechanisms of zoonotic severe acute respiratory syndrome coronavirus host range expansion in human airway epithelium. J. Virol. **82:**2274–2285.
27. **Sims, A. C., R. S. Baric, B. Yount, S. E. Burkett, P. L. Collins, and R. J. Pickles.** 2005. Severe acute respiratory syndrome coronavirus infection of human ciliated airway epithelia: role of ciliated cells in viral spread in the conducting airways of the lungs. J. Virol. **79:**15511–15524.
28. **ter Meulen, J., E. N. van den Brink, L. L. Poon, W. E. Marissen, C. S. Leung, F. Cox, C. Y. Cheung, A. Q. Bakker, J. A. Bogaards, E. van Deventer, W. Preiser, H. W. Doerr, V. T. Chow, J. de Kruif, J. S. Peiris, and J. Goudsmit.** 2006. Human monoclonal antibody combination against SARS coronavirus: synergy and coverage of escape mutants. PLoS Med. **3:**e237.
29. **Towner, J. S., X. Pourrut, C. G. Albarino, C. N. Nkogue, B. H. Bird, G. Grard, T. G. Ksiazek, J. P. Gonzalez, S. T. Nichol, and E. M. Leroy.** 2007. Marburg virus infection detected in a common African bat. PLoS ONE **2:**e764.
30. **Traggiai, E., S. Becker, K. Subbarao, L. Kolesnikova, Y. Uematsu, M. R. Gismondo, B. R. Murphy, R. Rappuoli, and A. Lanzavecchia.** 2004. An efficient method to make human monoclonal antibodies from memory B cells: potent neutralization of SARS coronavirus. Nat. Med. **10:**871–875.
31. **Woo, P. C., S. K. Lau, K. S. Li, R. W. Poon, B. H. Wong, H. W. Tsoi, B. C. Yip, Y. Huang, K. H. Chan, and K. Y. Yuen.** 2006. Molecular diversity of coronaviruses in bats. Virology **351:**180–187.
32. **Woo, P. C., S. K. Lau, and K. Y. Yuen.** 2006. Infectious diseases emerging from Chinese wet-markets: zoonotic origins of severe respiratory viral infections. Curr. Opin. Infect. Dis. **19:**401–407.
33. **Woo, P. C., M. Wang, S. K. Lau, H. Xu, R. W. Poon, R. Guo, B. H. Wong, K. Gao, H. W. Tsoi, Y. Huang, K. S. Li, C. S. Lam, K. H. Chan, B. J. Zheng, and K. Y. Yuen.** 2006. Comparative analysis of 12 genomes of three novel group 2c and group 2d coronaviruses reveals unique group and subgroup features. J. Virol. **81:**1574–1585.
34. **Wu, D., C. Tu, C. Xin, H. Xuan, Q. Meng, Y. Liu, Y. Yu, Y. Guan, Y. Jiang, X. Yin, G. Crameri, M. Wang, C. Li, S. Liu, M. Liao, L. Feng, H. Xiang, J. Sun, J. Chen, Y. Sun, S. Gu, N. Liu, D. Fu, B. T. Eaton, L. F. Wang, and X. Kong.** 2005. Civets are equally susceptible to experimental infection by two different severe acute respiratory syndrome coronavirus isolates. J. Virol. **79:**2620–2625.
35. **Xiao, Y., Q. Meng, X. Yin, Y. Guan, Y. Liu, C. Li, M. Wang, G. Liu, T. Tong, L. F. Wang, X. Kong, and D. Wu.** 2008. Pathological changes in masked palm civets experimentally infected by severe acute respiratory syndrome (SARS) coronavirus. J. Comp. Pathol. **138:**171–179.
36. **Yang, Z. Y., H. C. Werner, W. P. Kong, K. Leung, E. Traggiai, A. Lanzavecchia, and G. J. Nabel.** 2005. Evasion of antibody neutralization in emerging severe acute respiratory syndrome coronaviruses. Proc. Natl. Acad. Sci. USA **102:**797–801.
37. **Yount, B., K. M. Curtis, E. A. Fritz, L. E. Hensley, P. B. Jahrling, E. Prentice, M. R. Denison, T. W. Geisbert, and R. S. Baric.** 2003. Reverse genetics with a full-length infectious cDNA of severe acute respiratory syndrome coronavirus. Proc. Natl. Acad. Sci. USA **100:**12995–13000.
38. **Yount, B., R. S. Roberts, A. C. Sims, D. Deming, M. B. Frieman, J. Sparks, M. R. Denison, N. Davis, and R. S. Baric.** 2005. Severe acute respiratory

syndrome coronavirus group-specific open reading frames encode nonessential functions for replication in cell cultures and mice. J. Virol. **79:**14909–14922.

39. **Yu, S., M. Qiu, Z. Chen, X. Ye, Y. Gao, A. Wei, X. Wang, L. Yang, J. Wang, J. Wen, Y. Song, D. Pei, E. Dai, Z. Guo, C. Cao, J. Wang, and R. Yang.** 2005. Retrospective serological investigation of severe acute respiratory syndrome coronavirus antibodies in recruits from mainland China. Clin. Diagn. Lab. Immunol. **12:**552–554.
40. **Zheng, B. J., K. H. Wong, J. Zhou, K. L. Wong, B. W. Young, L. W. Lu, and S. S. Lee.** 2004. SARS-related virus predating SARS outbreak, Hong Kong. Emerg. Infect. Dis. **10:**176–178.
41. **Zhu, Z., S. Chakraborti, Y. He, A. Roberts, T. Sheahan, X. Xiao, L. E. Hensley, P. Prabakaran, B. Rockx, I. A. Sidorov, D. Corti, L. Vogel, Y. Feng, J. O. Kim, L. F. Wang, R. Baric, A. Lanzavecchia, K. M. Curtis, G. J. Nabel, K. Subbarao, S. Jiang, and D. S. Dimitrov.** 2007. Potent cross-reactive neutralization of SARS coronavirus isolates by human monoclonal antibodies. Proc. Natl. Acad. Sci. USA **104:**12123–12128.